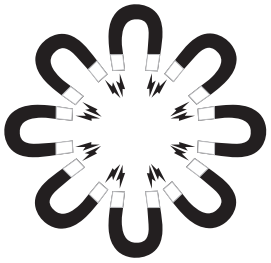
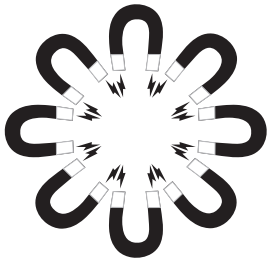

III Clinical applications of 7 Tesla MRI

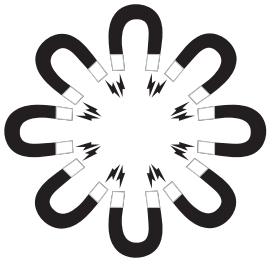
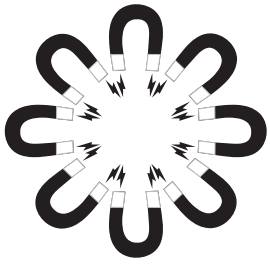

8

Cortical phase changes in Alzheimer's disease at 7 Tesla MRI: a novel imaging marker

S. van Rooden
M.J. Versluis
M.K. Liem
J. Milles
A.B. Maier
A.M.Oleksik
A.G. Webb
M.A. van Buchem
J. van der Grond

Under revision in Alzheimer's and Dementia

ABSTRACT

Background

Post mortem studies have indicated the potential of high-field magnetic resonance imaging (MRI) to visualize amyloid depositions in the cerebral cortex. The aim of this study is to test this hypothesis in patients with Alzheimer's disease (AD).

Methods

T_2^*- weighted MRI was performed in 15 AD patients and 16 control subjects. All MRI scans were scored qualitatively by visual assessment and quantitatively by measuring phase shifts in the cortical gray matter and hippocampus. Statistical analysis was performed to assess differences between groups.

Results

Patients with AD demonstrated an increased phase shift in the cortex in temporoparietal, frontal, and parietal regions ($p<0.005$) and this was associated with the individual Mini Mental State Examination ($r = -0.54$, $p<0.05$).

Discussion

Increased cortical phase shift in AD patients demonstrated on 7 Tesla T_2^*-weighted MRI is a potential new biomarker for AD, which may reflect amyloid pathology in the early stages.

INTRODUCTION

Alzheimer's disease (AD) can only be diagnosed with certainty at autopsy, based on the histological detection of senile plaques containing fibrillary amyloid-β (Aβ) and neurofibrillary tangles. Currently, due to the absence of validated sensitive and specific tests, the clinical diagnosis of AD can only be made at a late stage of disease progression and with a considerable degree of uncertainty, "probable AD" at best, and is based on criteria from the Diagnostic and Statistical Manual of Mental Disorders (DSM-IV) and the National Institute of Neurologic, Communicative Disorders and Stroke-AD and Related Disorders Association (NINCDS-ADRDA). Nevertheless, the histological hallmarks of AD pathology, comprising amyloid plaques and neurofibrillary tangles, are known to occur up to 10 to 20 years before the objective detection of cognitive decline (1). Recently, positron emission tomography (PET) using Pittsburgh compound-B (PiB) has been introduced as a diagnostic tool to detect cerebral amyloid in-vivo (2–8). The major disadvantages of PiB-PET are the need to use a radioactive tracer, the relative scarcity of institutions that can perform such scans due to the requirement for an on-site cyclotron, the inability to acquire anatomical and functional information in the brain during the same examination and the high prevalence of positive amyloid scans in asymptomatic individuals, especially in the elderly which hampers the use of this method as a diagnostic tool in the elderly (9).

Earlier research demonstrated the potential of high-field (7T) magnetic resonance imaging (MRI) in the diagnosis of AD by showing distinct intensity changes in the cortex on T_2^*-weighted images of post mortem brain specimens of AD patients. These features included hypointense foci and diffuse granular patterns of less distinct hypointense foci in the cerebral cortex (10). Similar patterns have been described in studies of AD transgenic mice and post mortem human AD, and were attributed to the presence of amyloid plaques using histological confirmation (11–19). It has been proposed that the visualization on MRI of plaques in humans and mice is based on the fact that these deposits co-localize with iron, which gives rise to magnetic susceptibility effects on T_2^*-weighted images over volumes that are much larger than the actual size of amyloid plaques (17, 19–24). An alternative method to measure these susceptibility changes in the brain is to measure the relative phase in regions of interest, since it has been shown that this is a reliable indicator of the iron content in the brain (25–28). Although previous studies have demonstrated the potential of this approach in high-field MRI (29, 30), no clinical studies have been performed yet on AD patients in-vivo for the detection of AD pathology.

The overall aim of the present study is to confirm previous post mortem findings, by detecting AD pathology in the cerebral cortex and hippocampus, using a novel in vivo 7T high-field MR approach.

MATERIALS AND METHODS

Participants

This study was approved by the local institutional review board. In all cases, informed consent was obtained according to the declaration of Helsinki (31). In total 16 AD patients with a mean age of 76.9 years (range 68 to 86 years, 10 male/6 female) and 15 control subjects with a mean age of 75.1 years (range 69 to 80 years, 10 male/5 female) were included.

The AD patients were recruited from the memory clinic of the Leiden University Medical Center. Memory clinic patients were referred to the hospital by their general practitioner or a medical specialist. Prior to the 7T study these patients all underwent a routine clinical protocol, comprising a whole brain MRI (3 Tesla), a battery of neuropsychological tests, and a general medical and neurological examination performed by a neurologist, psychiatrist or internist-geriatrician. The diagnosis was made in a multidisciplinary consensus meeting using the NINCDS-ADRDA criteria for diagnosing probable Alzheimer's disease (32). Participants with the diagnosis 'probable AD', who were capable of giving informed consent (Mini Mental State Examination (MMSE) ≥ 19) with late onset dementia (age > 67 year) were selected for inclusion in the 7T study either retrospectively within one year after attending the memory clinic, or prospectively.

Healthy control subjects were recruited by focussed advertisement. Subjects with an age between 69-80 years, who were living independently, had an MMSE ≥ 25 and a Geriatric Depression Scale (GDS) ≤ 4 were selected for inclusion. Subjects with the following diseases were excluded; stroke, morbus Parkinson, dementia, diabetes mellitus, rheumatoid arthritis, polymyalgia rheumatica, cancer, heart failure, and chronic obstructive pulmonary disease.

Image acquisition

MRI was performed on a whole body human 7 T MR system (Philips Healthcare, Best, the Netherlands) using a quadrature transmit and 16-channel receive head coil (Nova Medical, Wilmington, MA, USA). Participants were scanned using a 2D flow-compensated transverse T_2^*-weighted gradient-echo scan which included the frontal and parietal regions for amyloid detec-

tion with a total imaging duration of 10 minutes. Imaging parameters were: repetition time (TR)/echo time (TE) 794/25 ms, flip angle 45°, slice thickness 1.0 mm with a 0.1 mm interslice gap, 20 slices, 240 x 180 x 22 mm field of view, 1000 x 1024 matrix size – resulting in an in-plane nominal spatial resolution of 0.24 x 0.24 mm^2. Figure 1 shows a typical positioning of these 20 slices. The bandwidth per pixel was 46 Hz, corresponding to a readout length of approximately 22 ms. The frequency and phase encoding directions were along the anterior-posterior and right-left axes, respectively. Additionally, a coronal 2D flow-compensated T_2^*-weighted gradient echo scan covering the hippocampus with a total imaging duration of 6 minutes was performed. Imaging parameters were: TR/TE 624/14 ms, flip angle of 40°, slice thickness of 3.0 mm with no interslice gap, 32 slices, 240 x 180 x 96 mm field of view, 480 x 480 matrix size - resulting in a nominal in-plane spatial resolution of 0.5 x 0.5 mm^2. These sequences are very sensitive to image artifacts arising from resonance frequency fluctuations within the brain caused by slight patient movements, even in areas significantly away from the head. A navigator echo was included to correct for these artifacts (33). Shimming up to third order was performed using an image based shimming approach (34). The phase images were subsequently unwrapped by highpass filtering with a 92x92 kernel size (35).

Image analysis

First, the T_2^*-weighted gradient-echo images were evaluated, blinded for diagnosis, for hypointense foci by SvR and checked by MvB as described in a previous ex-vivo study (10).

Image phase values in the cortex were determined using the transverse 2D T_2^*-weighted gradient echo scans. Based on the visual observation on unwrapped phase images of a higher contrast between gray and white matter in AD patients than in controls, due to a higher signal intensity within the gray matter, the phase values of the cortical gray matter were determined in regions of interest (ROIs) in four different areas of the brain: temporoparietal left, temporoparietal right, frontal and parietal. Because of the laminar variation in the cortical areas (29), histograms perpendicular to the cortex within these regions were created to measure peak gray matter phase values, over at least 10 cortical regions per slice and per region. To correct for local macroscopic magnetic field inhomogeneities subcortical white matter phase values were measured and used as an internal reference value. Phase values for gray and white matter were measured in these four areas per MRI slice for every other slice (ten in total), resulting in 40 phase values for gray and white matter separately per subject. Phase values of the different ROIs of the four

regions were averaged. Per subject, the overall phase shift between cortical gray and subcortical white matter (cortical phase shift) was calculated for each region and expressed in radians.

Phase values of the hippocampus were determined using the coronal 2D T_2^*-weighted gradient echo scans. The hippocampus was manually segmented and phase values were determined on 5 consecutive slices, starting at the head of the hippocampus, for the right and left hippocampus separately. For each subject, these five measurements were averaged for each hippocampus. Phase values of the white matter were determined in three neighboring areas of subcortical white matter on each of the five slices and averaged per subject. The phase shift of the hippocampus was calculated by the difference in phase value of the hippocampus and white matter (hippocampal phase shift) and expressed in radians. Analysis of the hippocampus was only performed in 12 of the 16 AD patients and in 14 of the 15 controls, because of severe motion artifacts that could not be completely corrected for (three subjects) or because participants were not able to finish the whole scan protocol (two subjects).

Statistics

A Mann-Whitney U-test was used to assess differences in age, gender, MMSE and phase measurements between AD and control groups. Logistic regression analysis was used to assess the association between diagnosis and intertissue phase shifts in the cortex and hippocampus, corrected for age and gender. To assess the interaction between cortical gray matter/hippocampal and white matter phase values, both were also entered as covariates in one model. Receiver operating characteristic (ROC) analysis was performed to determine the area under the ROC curve and to assess the optimal cut-off phase shift in the cortex and hippocampus to detect AD with its corresponding sensitivity, specificity, positive predictive value, and negative predictive value. To determine the association between MMSE and phase shift in the cortex and hippocampus, a linear regression analysis including a Pearson correlation corrected for age and gender was performed. All statistical analyses were performed with the Statistical Package of Social Sciences (SPSS, version 17.0.1; SPSS, Chicago, Ill).

RESULTS

The characteristics of the participants are shown in Table 1. No difference in age or gender was found between patient and control groups. Scores for global cognitive functioning (MMSE score) were significantly higher in controls

(29.0 points) than in patients with AD (22.5 points), p<0.001.

Table 1: Characteristics of AD patients and control subjects.		
	AD (n = 16)	Controls (n = 15)
Mean age, years (range)	76.9 (68–86)	75.1 (69–80)
Male/female	10/6	10/5
Median MMSE, points (range)	22.5 (19-26)	29.0 (27-30)

AD = Alzheimer's Disease, MMSE = Mini Mental State Examination.

Figure 2 shows representative transverse T_2*-weighted magnitude and phase images of the parietal region of a subject with AD (a and b) and a control subject (c and d). Figure 3 shows coronal T_2*-weighted magnitude and phase images of the hippocampus of a subject with AD (a and b) and a control subject (c and d). In none of the subjects were small focal hypointensities found in either the cortex or hippocampus.

Table 2: Mean phase differences and SDs of the cortical and hippocampal subregions in AD patients and control subjects.			
	AD (rad) (n = 16)	Control (rad) (n = 15)	p-value
Temporoparietal left	0.90 ± 0.08	0.79 + 0.08	0.001
Temporoparietal right	0.97 + 0.10	0.85 + 0.09	0.001
Frontal	0.70 ± 0.08	0.62 ± 0.07	0.004
Parietal	0.87 ± 0.10	0.74 ± 0.08	0.000
Hippocampus right	0.09 ± 0.04	0.07 ± 0.03	0.18
Hippocampus left	0.10 ± 0.04	0.08 ± 0.02	0.14

AD = Alzheimer's Disease, rad = radians.

Table 2 shows the mean phase shifts of the temporoparietal, frontal, parietal cortex and the right and left hippocampus. For the temporoparietal, frontal, and parietal cortex, a larger cortical phase shift (p <0.005) was found in the AD patients compared to control subjects (adjusted for age and gender). For both hippocampi no difference in phase shifts between groups was observed. Analysis in which both gray and white matter values were entered in the logistic regression model showed that only the cortical gray matter phase value, and not the white matter phase value, was associated with diagnosis. For the hippocampus, both gray and white matter phase values were not associated with diagnosis.

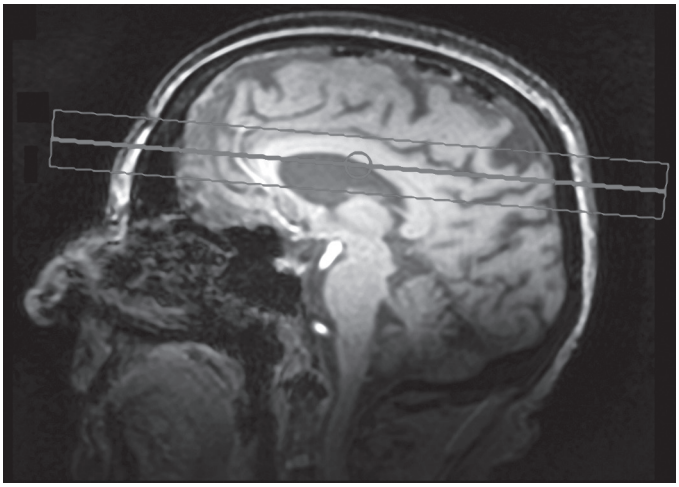

Figure 1: Sagittal survey image.
The stack position of the 2D T_2*-weighted gradient-echo scan including the frontal and parietal regions for amyloid detection is shown. Image shows sagittal plane.

To determine the diagnostic value of the phase measurements in differentiating AD from control subjects, ROC analysis was performed for each region. Table 3 shows the area under the curve (AUC), cut-off value, sensitivity, specificity, positive and negative predictive values of all regions selected. For the temporoparietal, frontal, and parietal cortex an AUC between 0.79 and 0.85 was found, with the regions all having a high specificity (90-100%) and a moderate-to-high sensitivity (50-70%). Of these regions, the parietal cortex demonstrated the highest AUC (0.85) with a sensitivity of 69% and a specificity of 93%. The corresponding positive predictive value and negative predictive value were 92% and 74%. Both hippocampi demonstrated a lower AUC; right hippocampus 0.66 and left hippocampus 0.67. This resulted in a relatively lower specificity and positive predictive value. The sensitivity and negative predictive values were comparable with the regions in the cortex.

There was a significant negative correlation (adjusted for age and gender) between MMSE and phase shift in the left temporoparietal cortex, r = -0.47 (β = -0.464, p<.05), the right temporoparietal cortex, r = -0.41 (β = -0.473, p<.05), frontal cortex, r = -0.44 (β = -0.404, p<.05) and parietal cortex, r = -0.54 (β = -0.501, p<.05) (all: P < 0.05). For the right and the left hippocampus there was no correlation between MMSE and phase shift (right hippocampus, r = -0.25, p = 0.21 (β = -0.168, p = .404), left hippocampus, r = -0.27, p = 0.19 (β = -0.190, p = .336)).

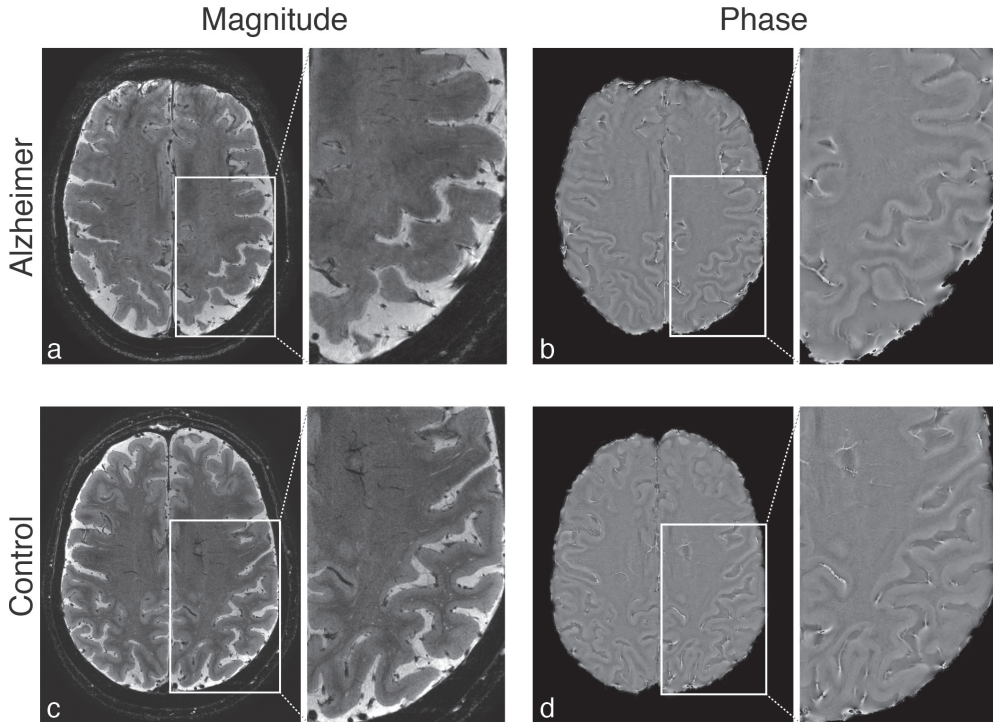

Figure 2: Cortex T_2^*-weighted images obtained in AD patient and control subject.
Representative 0.24 x 0.24 mm^2 2D T_2*- weighted gradient echo images show an AD patient (A and B) and a control subject (C and D). Image A and C show magnitude images and image B and D phase images of the parietal region. No hypointense foci are seen on the magnitude images. The phase images show that the contrast between gray and white matter is enhanced in the AD patient in comparison to the control subject, indicating a larger cortical phase difference. Images show transverse planes.

DISCUSSION

This study shows that using a novel high-field imaging approach at 7T, patients with clinical symptoms of AD demonstrate an increased cortical phase shift on T_2^*-weighted images. These phase shifts between AD patients and control subjects have a high specificity, independent of age and gender. Moreover, these phase shifts correlated with individual MMSE scores. Of all cortical areas studied, the parietal cortex shows the highest specificity combined with the highest sensitivity for the diagnosis AD and the strongest correlation with MMSE. On the other hand, phase shifts in the hippocampus were not significantly increased in AD patients and did not correlate with MMSE.

High-field T_2^*-weighted MRI sequences are highly sensitive for iron depos-

its in the brain (36). In autopsy material of AD patients amyloid deposition and neurofibrillary tangles as well as tau deficiency were found to co-localize with neuronal iron accumulation (37–39). Therefore, it is likely that the increased cortical phase shift found on high-field T_2^*-weighted MRI in patients with AD indirectly reflect AD pathology. Our data also show that the particular distribution of the phase changes in the brain follows the known cerebral distribution of amyloid deposition in AD. In our data the neocortex, and more specifically the parietal lobes, allowed much better differentiating of AD patients from control subjects based on phase shift as compared to the hippocampus. In histological studies it was demonstrated that the neocortex is the first structure in the brain that is affected by amyloid depositions whereas the hippocampus is not only more mildly affected by amyloid plaques but also affected at a later stage of AD than the neocortex (40–42). This sequence of events has been confirmed by PiB-PET studies, showing high amyloid loads in the parietal and frontal lobes and not in hippocampus (5–7, 43, 44).

Phase measurement on T_2^*-weighted MRI at 7 Tesla has a high specificity for AD as compared to the reported specificity of the methods that are currently considered state of the art, such as cerebrospinal fluid (CSF) assay of the amyloid peptide or PiB PET imaging (9). Previous studies indicated that AD patients have reduced levels of Aβ1-42 and increased levels of t-tau and p-tau181p in CSF compared to control subjects of which Aβ1-42 is the most sensitive biomarker for AD of CSF samples. 7T MRI had lower sensitivity than these CSF analyses of Aβ1-42 (69% vs. 96%) but had a higher specificity (93-100% vs. 77%) (45). PET studies using [11C] Pittsburgh Compound-B (PiB-PET) have shown the possibility of detecting cerebral amyloid accumulation, although the diagnostic utility is limited (46) and numbers on sensitivity and specificity are sparse. Mormino and coworkers (47) showed high sensitivity (90%) and specificity (90%) in differentiating AD patients from controls. However, within the group of healthy subjects the specificity drops with increasing age, because the percentage of positive PiB-PET scans increases rapidly with 12% of the people in their 60s, 30% in their 70s and 50% in their 80s giving “false positive” results (44, 48, 49). Our data show that measurement of phase shift using T_2^*-weighted MRI might improve the specificity of AD diagnosis.

Our study could not replicate the ex-vivo finding of hypointense foci, that might represent amyloid plaques (10). Although we corrected for resonance frequency variations, which are the main contributor to decreased image quality in AD patients, with a navigator echo (33) it is highly likely that even

sub-voxel degrees of motion blur the hypointense foci.

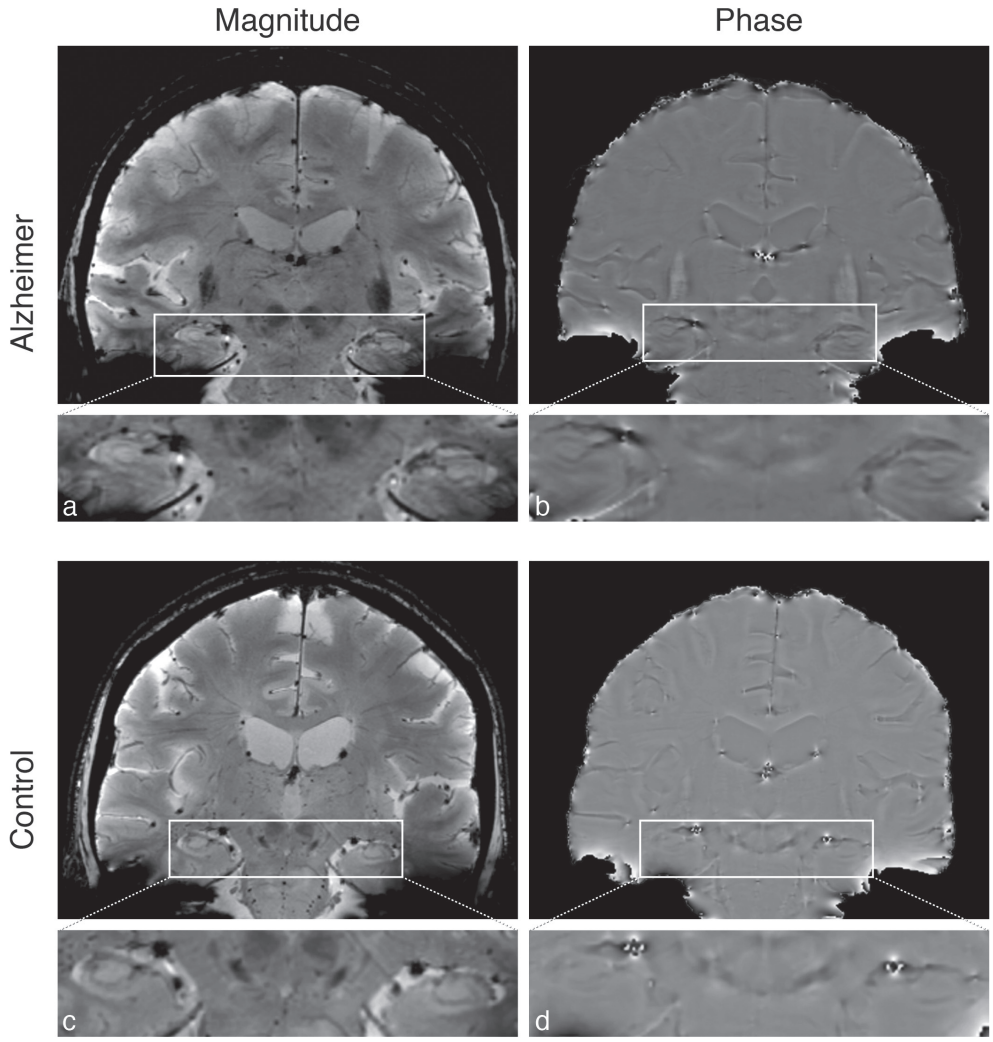

Figure 3: Hippocampus T_2^*-weighted images obtained in AD patient and control subject. Representative 0.5 x 0.5 mm^2 2D T_2^*- weighted gradient echo images show an AD patient (A and B) and a control subject (C and D). Image A and C show magnitude images and image B and D phase images of the hippocampal region. No hypointense foci are seen on the magnitude images. The phase images show no difference between the AD patient and the control subject in terms of image contrast between hippocampus and white matter.

Table 3: differentiating between AD patients and control subjects for the different regions.						
	AUC	cut-off value (rad)	Sensitivity (%)	Specificity (%)	PPV+ (%)	NPV-(%)
Temporoparietal left	0.842	0.922	56 (9/16)	100 (15/15)	100 (9/9)	68 (15/22)
Temporoparietal right	0.823	0.985	50 (8/16)	100 (15/15)	100 (8/8)	65 (15/23)
Frontal	0.794	0.690	56 (9/16)	93 (14/15)	90 (9/10)	67 (14/21)
Parietal	0.854	0.817	69 (11/16)	93 (14/15)	92 (11/12)	74 (14/19)
Hippocampus right	0.655	0.074	75 (9/12)	71 (10/14)	69 (9/13)	77 (10/13)
Hippocampus left	0.673	0.095	58 (7/12)	86 (12/14)	78 (7/9)	71 (12/17)

AUC = area under the curve, PPV+ = positive predictive value, NPV- = negative predictive value.

A limitation of the present study is that phase measurements might also be influenced by the geometry and orientation of the scans (28). We limited these effects as much as possible by carefully positioning every participant in the same manner. Moreover, phase values were measured in the exact same way by using a standardized method. Furthermore, we averaged multiple measurements of phase values to cancel out the possible effects of geometry and orientation. A second limitation is that white matter phase values, which were used to correct for magnetic field inhomogeneities, might have an influence on the results. However, our data show that the observed phase changes were mainly caused by phase shifts in the gray matter. A third limitation is that we only included AD patients and healthy controls and therefore the diagnostic accuracy of our method in a group of memory clinic patients is unclear. The specificity of the presented method should be examined thoroughly by assessing different categories of neurodegenerative diseases to evaluate the ability to differentiate between different forms of dementia. Moreover, the value of our method should be investigated in the preclinical stages of AD in future studies to evaluate the possibility of detecting early AD pathology and to be used as an early treatment marker.

In conclusion, in this study we introduced a novel approach to detect cortical changes in AD patients exploiting the increased sensitivity of 7T MRI for iron in brain tissue. Our current data demonstrate that cortical phase changes are a potential new biomarker for AD.

ACKNOWLEDGEMENTS

This research was performed within the framework of CTMM, the Center for Translational Molecular Medicine (www.ctmm.nl), project LeARN (grant 02N-101) and was supported by NGI/NWO (05040202, 050-060-810) and HEALTH-2007-2.4.5-10.

REFERENCES

1. Nelson PT, Braak H, Markesbery WR. Neuropathology and cognitive impairment in Alzheimer disease: a complex but coherent relationship. J. Neuropathol. Exp. Neurol. 2009 ;68:1–14.
2. Johnson KA, Gregas M, Becker JA, Kinnecom C, Salat DH, Moran EK, Smith EE, Rosand J, Rentz DM, Klunk WE, Mathis CA, Price JC, Dekosky ST, Fischman AJ, Greenberg SM. Imaging of amyloid burden and distribution in cerebral amyloid angiopathy. Ann. Neurol. 2007 ;62:229–234.
3. Lockhart A, Lamb JR, Osredkar T, Sue LI, Joyce JN, Ye L, Libri V, Leppert D, Beach TG. PIB is a non-specific imaging marker of amyloid-beta (Abeta) peptide-related cerebral amyloidosis. Brain 2007 ;130:2607–2615.
4. Ikonomovic MD, Klunk WE, Abrahamson EE, Mathis CA, Price JC, Tsopelas ND, Lopresti BJ, Ziolko S, Bi W, Paljug WR, Debnath ML, Hope CE, Isanski BA, Hamilton RL, DeKosky ST. Post-mortem correlates of in vivo PiB-PET amyloid imaging in a typical case of Alzheimer's disease. Brain 2008 ;131:1630–1645.
5. Klunk WE, Engler H, Nordberg A, Wang Y, Blomqvist G, Holt DP, Bergström M, Savitcheva I, Huang G-F, Estrada S, Ausén B, Debnath ML, Barletta J, Price JC, Sandell J, Lopresti BJ, Wall A, Koivisto P, Antoni G, Mathis CA, Långström B. Imaging brain amyloid in Alzheimer's disease with Pittsburgh Compound-B. Annals of Neurology 2004 ;55:306–319.
6. Engler H, Forsberg A, Almkvist O, Blomquist G, Larsson E, Savitcheva I, Wall A, Ringheim A, Långström B, Nordberg A. Two-year follow-up of amyloid deposition in patients with Alzheimer's disease. Brain 2006 ;129:2856–2866.
7. Rowe CC, Ng S, Ackermann U, Gong SJ, Pike K, Savage G, Cowie TF, Dickinson KL, Maruff P, Darby D, Smith C, Woodward M, Merory J, Tochon-Danguy H, O'Keefe G, Klunk WE, Mathis CA, Price JC, Masters CL, Villemagne VL. Imaging beta-amyloid burden in aging and dementia. Neurology 2007 ;68:1718–1725.
8. Bacskai BJ, Frosch MP, Freeman SH, Raymond SB, Augustinack JC, Johnson KA, Irizarry MC, Klunk WE, Mathis CA, Dekosky ST, Greenberg SM, Hyman BT, Growdon JH. Molecular imaging with Pittsburgh Compound B confirmed at autopsy: a case report. Arch. Neurol. 2007 ;64:431–434.
9. Rowe CC, Villemagne VL. Brain amyloid imaging. J. Nucl. Med. 2011 ;52:1733–1740.
10. van Rooden S, Maat-Schieman MLC, Nabuurs RJA, van der Weerd L, van Duijn S, van Duinen SG, Natté R, van Buchem MA, van der Grond J. Cerebral amyloidosis: postmortem detection with human 7.0-T MR imaging system. Radiology 2009 ;253:788–796.
11. Benveniste H, Einstein G, Kim KR, Hulette C, Johnson GA. Detection of neuritic plaques in Alzheimer's disease by magnetic resonance microscopy. Proc. Natl. Acad. Sci. U.S.A. 1999 ;96:14079–14084.
12. Zhang J, Yarowsky P, Gordon MN, Di Carlo G, Munireddy S, van Zijl PCM, Mori S. Detection of amyloid plaques in mouse models of Alzheimer's disease by magnetic resonance imaging. Magn Reson Med 2004 ;51:452–457.
13. Helpern JA, Lee S-P, Falangola MF, Dyakin VV, Bogart A, Ardekani B, Duff K, Branch C, Wisniewski T, de Leon MJ, Wolf O, O'Shea J, Nixon RA. MRI assessment of neuropathology in a transgenic mouse model of Alzheimer's disease. Magn Reson Med 2004 ;51:794–798.

14. Lee S-P, Falangola MF, Nixon RA, Duff K, Helpern JA. Visualization of beta-amyloid plaques in a transgenic mouse model of Alzheimer's disease using MR microscopy without contrast reagents. Magn Reson Med 2004 ;52:538–544.
15. Jack CR Jr, Garwood M, Wengenack TM, Borowski B, Curran GL, Lin J, Adriany G, Gröhn OHJ, Grimm R, Poduslo JF. In vivo visualization of Alzheimer's amyloid plaques by magnetic resonance imaging in transgenic mice without a contrast agent. Magn Reson Med 2004 ;52:1263–1271.
16. Braakman N, Matysik J, van Duinen SG, Verbeek F, Schliebs R, de Groot HJM, Alia A. Longitudinal assessment of Alzheimer's beta-amyloid plaque development in transgenic mice monitored by in vivo magnetic resonance microimaging. J Magn Reson Imaging 2006 ;24:530–536.
17. Vanhoutte G, Dewachter I, Borghgraef P, Van Leuven F, Van der Linden A. Noninvasive in vivo MRI detection of neuritic plaques associated with iron in APP[V717I] transgenic mice, a model for Alzheimer's disease. Magn Reson Med 2005 ;53:607–613.
18. Nakada T, Matsuzawa H, Igarashi H, Fujii Y, Kwee IL. In vivo visualization of senile-plaque-like pathology in Alzheimer's disease patients by MR microscopy on a 7T system. J Neuroimaging 2008 ;18:125–129.
19. Meadowcroft MD, Connor JR, Smith MB, Yang QX. MRI and histological analysis of beta-amyloid plaques in both human Alzheimer's disease and APP/PS1 transgenic mice. J Magn Reson Imaging 2009 ;29:997–1007.
20. Falangola MF, Lee S-P, Nixon RA, Duff K, Helpern JA. Histological co-localization of iron in Abeta plaques of PS/APP transgenic mice. Neurochem. Res. 2005 ;30:201–205.
21. Grundke-Iqbal I, Fleming J, Tung YC, Lassmann H, Iqbal K, Joshi JG. Ferritin is a component of the neuritic (senile) plaque in Alzheimer dementia. Acta Neuropathol. 1990 ;81:105–110.
22. El Tannir El Tayara N, Delatour B, Le Cudennec C, Guégan M, Volk A, Dhenain M. Age-related evolution of amyloid burden, iron load, and MR relaxation times in a transgenic mouse model of Alzheimer's disease. Neurobiol. Dis. 2006 ;22:199–208.
23. Exley C. Aluminium and iron, but neither copper nor zinc, are key to the precipitation of beta-sheets of Abeta_{42} in senile plaque cores in Alzheimer's disease. J. Alzheimers Dis. 2006 ;10:173–177.
24. Lovell MA, Robertson JD, Teesdale WJ, Campbell JL, Markesbery WR. Copper, iron and zinc in Alzheimer's disease senile plaques. J. Neurol. Sci. 1998 ;158:47–52.
25. Ogg RJ, Langston JW, Haacke EM, Steen RG, Taylor JS. The correlation between phase shifts in gradient-echo MR images and regional brain iron concentration. Magn Reson Imaging 1999 ;17:1141–1148.
26. Haacke EM, Cheng NYC, House MJ, Liu Q, Neelavalli J, Ogg RJ, Khan A, Ayaz M, Kirsch W, Obenaus A. Imaging iron stores in the brain using magnetic resonance imaging. Magnetic Resonance Imaging 2005 ;23:1–25.
27. Haacke EM, Ayaz M, Khan A, Manova ES, Krishnamurthy B, Gollapalli L, Ciulla C, Kim I, Petersen F, Kirsch W. Establishing a baseline phase behavior in magnetic resonance imaging to determine normal vs. abnormal iron content in the brain. Journal of Magnetic Resonance Imaging: JMRI 2007 ;26:256–64.
28. Yao B, Li T-Q, Gelderen P van, Shmueli K, de Zwart JA, Duyn JH. Susceptibility contrast in high field MRI of human brain as a function of tissue iron content. NeuroImage 2009 ;44:1259–1266.

29. Duyn JH, van Gelderen P, Li T-Q, de Zwart JA, Koretsky AP, Fukunaga M. High-field MRI of brain cortical substructure based on signal phase. Proceedings of the National Academy of Sciences 2007 ;104:11796–11801.
30. Fukunaga M, Li T-Q, van Gelderen P, de Zwart JA, Shmueli K, Yao B, Lee J, Maric D, Aronova MA, Zhang G, Leapman RD, Schenck JF, Merkle H, Duyn JH. Layer-specific variation of iron content in cerebral cortex as a source of MRI contrast. Proceedings of the National Academy of Sciences 2010 ;107:3834 –3839.
31. Lynöe N, Sandlund M, Dahlqvist G, Jacobsson L. Informed consent: study of quality of information given to participants in a clinical trial. BMJ 1991 ;303:610–613.
32. McKhann G, Drachman D, Folstein M, Katzman R, Price D, Stadlan EM. Clinical diagnosis of Alzheimer's disease: report of the NINCDS-ADRDA Work Group under the auspices of Department of Health and Human Services Task Force on Alzheimer's Disease. Neurology 1984 ;34:939–944.
33. Versluis MJ, Peeters JM, van Rooden S, van der Grond J, van Buchem MA, Webb AG, van Osch MJP. Origin and reduction of motion and f0 artifacts in high resolution T2*-weighted magnetic resonance imaging: Application in Alzheimer's disease patients. NeuroImage 2010 ;51:1082–1088.
34. Schär M, Kozerke S, Fischer SE, Boesiger P. Cardiac SSFP imaging at 3 Tesla. Magnetic Resonance in Medicine 2004 ;51:799–806.
35. Haacke EM, Xu Y, Cheng Y-CN, Reichenbach JR. Susceptibility weighted imaging (SWI). Magnetic Resonance in Medicine 2004 ;52:612–618.
36. Duyn JH. The future of ultra-high field MRI and fMRI for study of the human brain. Neuroimage 2012 ;62:1241–1248.
37. Duce JA, Tsatsanis A, Cater MA, James SA, Robb E, Wikhe K, Leong SL, Perez K, Johanssen T, Greenough MA, Cho H-H, Galatis D, Moir RD, Masters CL, McLean C, Tanzi RE, Cappai R, Barnham KJ, Ciccotosto GD, Rogers JT, Bush AI. Iron-export ferroxidase activity of β-amyloid precursor protein is inhibited by zinc in Alzheimer's disease. Cell 2010 ;142:857–867.
38. Lei P, Ayton S, Finkelstein DI, Spoerri L, Ciccotosto GD, Wright DK, Wong BXW, Adlard PA, Cherny RA, Lam LQ, Roberts BR, Volitakis I, Egan GF, McLean CA, Cappai R, Duce JA, Bush AI. Tau deficiency induces parkinsonism with dementia by impairing APP-mediated iron export. Nat. Med. 2012 ;18:291–295.
39. Smith MA, Harris PL, Sayre LM, Perry G. Iron accumulation in Alzheimer disease is a source of redox-generated free radicals. Proc. Natl. Acad. Sci. U.S.A. 1997 ;94:9866–9868.
40. Braak H, Braak E. Neuropathological stageing of Alzheimer-related changes. Acta Neuropathol. 1991 ;82:239–259.
41. Arnold SE, Hyman BT, Flory J, Damasio AR, Van Hoesen GW. The topographical and neuroanatomical distribution of neurofibrillary tangles and neuritic plaques in the cerebral cortex of patients with Alzheimer's disease. Cereb. Cortex 1991 ;1:103–116.
42. Thal DR, Rüb U, Orantes M, Braak H. Phases of A beta-deposition in the human brain and its relevance for the development of AD. Neurology 2002 ;58:1791–1800.
43. Ng SY, Villemagne VL, Masters CL, Rowe CC. Evaluating atypical dementia syndromes using positron emission tomography with carbon 11 labeled Pittsburgh Compound B. Arch. Neurol. 2007 ;64:1140–1144.

44. Mintun MA, LaRossa GN, Sheline YI, Dence CS, Lee SY, Mach RH, Klunk WE, Mathis CA, DeKosky ST, Morris JC. [11C]PIB in a Nondemented Population Potential Antecedent Marker of Alzheimer Disease. Neurology 2006 ;67:446–452.
45. Shaw LM, Vanderstichele H, Knapik-Czajka M, Clark CM, Aisen PS, Petersen RC, Blennow K, Soares H, Simon A, Lewczuk P, Dean R, Siemers E, Potter W, Lee VM-Y, Trojanowski JQ. Cerebrospinal fluid biomarker signature in Alzheimer's disease neuroimaging initiative subjects. Ann. Neurol. 2009 ;65:403–413.
46. Quigley H, Colloby SJ, O'Brien JT. PET imaging of brain amyloid in dementia: a review. Int J Geriatr Psychiatry 2011 ;26:991–999.
47. Mormino EC, Kluth JT, Madison CM, Rabinovici GD, Baker SL, Miller BL, Koeppe RA, Mathis CA, Weiner MW, Jagust WJ. Episodic memory loss is related to hippocampal-mediated beta-amyloid deposition in elderly subjects. Brain 2009 ;132:1310–1323.
48. Rowe CC, Ellis KA, Rimajova M, Bourgeat P, Pike KE, Jones G, Fripp J, Tochon-Danguy H, Morandeau L, O'Keefe G, Price R, Raniga P, Robins P, Acosta O, Lenzo N, Szoeke C, Salvado O, Head R, Martins R, Masters CL, Ames D, Villemagne VL. Amyloid imaging results from the Australian Imaging, Biomarkers and Lifestyle (AIBL) study of aging. Neurobiol. Aging 2010 ;31:1275–1283.
49. Villemagne VL, Pike KE, Chételat G, Ellis KA, Mulligan RS, Bourgeat P, Ackermann U, Jones G, Szoeke C, Salvado O, Martins R, O'Keefe G, Mathis CA, Klunk WE, Ames D, Masters CL, Rowe CC. Longitudinal assessment of Aβ and cognition in aging and Alzheimer disease. Ann. Neurol. 2011 ;69:181–192.